# Resilient Scheduling Optimization of Multi-Energy Complementary Systems under Extreme Heat

Liangyu Tang, Yang Han, *Senior* Member, *IEEE*, Qirui Li, Chaofeng Yan, Meng Zhou and Yunfei Xue

***Abstract*—With the intensification of global climate change, extreme heat events pose multiple challenges to power systems, including surging load demand, reduced generation efficiency, and decreased transmission capacity. To address these issues, this paper proposes an optimization scheduling model for multi-energy complementary systems (MECS) under extreme heat conditions and develops a resilience evaluation framework combining Analytic Hierarchy Process (AHP) and Entropy Weight Method (EWM). A hierarchical load shedding strategy is designed, and demand response mechanisms are implemented. As a result, the system resilience index improves from 0.2 to 0.4329, enhancing system stability under extreme conditions.**

***Index Terms*—Extreme heat, multi-energy complementary system, resilience, demand response, vulnerability.**

## NOMENCLATURE

### *A. Constants*

| | |
|---|---|
| $P^{0,\mathrm{PV}}$ | Rated power of PV under standard conditions |
| $\delta_p$ | Temperature-power coefficient |
| $c_1/c_2/c_3/c_4$ | Coefficients related to PV operating temperature |
| $T_{health\_air}$ | Temperature when waste heat discharge is within normal operating range |
| $c_{shift}$ | Subsidy cost per MWh for shiftable load |
| $T$ | Total scheduling periods |
| $c_{int}$ | Subsidy cost per MWh for curtailable load |
| $N$ | Total number of curtailable nodes |
| $p_{t,ESS}^{grid}/p_{t,g}^{grid}$ | Feed-in tariff for energy storage/thermal power |
| $\eta_c$, $\eta_d$ | Charging/discharging efficiency of energy storage |
| $a_i$, $b_i$, $c_i$ | Quadratic/linear/constant coefficients for thermal power fuel cost |
| $S_i^{start}/S_i^{stop}$ | Start-up/shut-down costs for thermal power unit |
| $p_w/p_v/p_h$ | Feed-in tariff for wind/PV/hydropower |
| $\theta_w/\theta_v/\theta_h$ | Penalty for curtailed wind/ PV /hydropower |
| $P_{i,t}^{shed}$ | Base penalty cost for direct load shedding |
| $\delta$ | Self-discharge rate of energy storage |
| $E_{ESS}$ | Energy storage capacity |
| $S_{max}/S_{min}$ | Upper/lower limit of energy storage |
| $\lambda$ | Reserve coefficient |
| $P_{i,t,max}^{shift}/P_{i,t,max}^{int}$ | Maximum capacity of shiftable/ curtailable load |

### *B. Variables*

| | |
|---|---|
| $P_t^{PV}$ | Photovoltaic output power |
| $I_t$, $I^0$ | Actual/standard radiation intensity |
| $T^{\mathrm{air}}/T_t^{PV}/T^{0,\mathrm{PV}}$ | Air temperature/actual operating temperature/standard operating temperature |
| $v_t$ | Ground wind speed |
| $\rho$ | Efficiency degradation rate of thermal units |
| $T_j/T_j^{ref}$ | Actual temperature/historical reference temperature |
| $I$ | Allowable current capacity of transmission lines |
| $W_R/W_F/W_S$ | Radiative/convective heat dissipation/solar absorption power |
| $R'_t$ | AC resistance of the conductor |
| $P_t^{shift}$ | Shiftable load power |
| $P_t^{int}$ | Curtailable load power |
| $U_{i,t}$ | Load shedding state variable |
| $S_{i,t}$ | Curtailable load capacity |
| $P_g/P_w/P_v/P_h/P_{ESS}$ | Revenue from thermal/wind/photovoltaic/hydropower/ storage |
| $C_{DR}/C_{shed}$ | Demand response subsidy cost/direct load shedding cost |
| $P_t^{char}/P_t^{dis}$ | Charging/discharging power of energy storage |
| $C_g/I_g$ | Operating cost/revenue of thermal power |
| $P_{i,t}^g$ | Output of thermal unit |
| $C_{coal}/C_{ss}$ | Coal consumption/start-stop cost of units |
| $U_{i,t}^g$ | Start-stop state variable of thermal unit |
| $P_t^w/P_t^v/P_t^h$ | Output power of wind/photovoltaic/ hydropower |
| $P_{t,cur}^w/P_{t,cur}^v/P_{t,cur}^h$ | Curtailed wind/photovoltaic/hydropower |
| $C_{shift}/C_{int}$ | Subsidy cost for shiftable/ curtailable load |
| $P_{i,t}^{shed}$ | Direct load shedding power |
| $c_{i,t}^{shed}$ | Penalty coefficient for direct load shedding |
| $P_{t,max}^w/P_{t,max}^v/P_{t,max}^h$ | Output upper limits of wind/photovoltaic/hydropower |
| $U_t^g$ | Thermal unit output state variable |
| $P_{t,max}^g/P_{t,min}^g$ | Upper/lower limits of thermal unit output |
| $r_{i,up}/r_{i,down}$ | Max ramp-up/ramp-down rates of thermal units |
| $S_t^{ESS}$ | State of charge of energy storage |
| $S_0^{ESS}/S_T^{ESS}$ | State of charge at start/end of scheduling |
| $U_t^{char}/U_t^{dis}$ | Charging/discharging state variable of energy storage |
| $P_{max}^{char}/P_{min}^{char}$ | Upper/lower limits of charging power |
| $P_{max}^{dis}/P_{min}^{dis}$ | Upper/lower limits of discharging power |
| $B_{i,j}(S)$ | Susceptance |
| $\theta_{i,t}$, $\theta_{j,t}$ | Voltage angles |
| $P_{i,j,\mathrm{Lmax}}$ | Per-unit limit of line transmission power |
| $\alpha_{t,l}^{temp}/\beta_{t,l}^{temp}$ | Line/transformer capacity degradation factors |
| $P_{i,l,in}^{shift}/P_{i,l,out}^{shift}$ | Shiftable load power in/out |
| $P_{i,t}^{int}/P_{i,t}^{shed}$ | Curtailable /direct load shedding power |
| $P_{i,t,max}^g$ | Upper limit of thermal unit output |

## I. INTRODUCTION

Extreme weather events have increasingly occurred with greater frequency and intensity in recent years, posing significant risks to power system reliability and efficiency [1]. Among these events, extreme heat has become a global challenge, significantly affecting power systems. For example, during the summer of 2021, Europe experienced severe heatwaves, leading to surging electricity demand in countries such as France and Spain. Simultaneously, thermal power plant efficiency declined, and some nuclear power plants were forced to shut down [2]. Similarly, during the summer of 2022 in Southwest China, record-breaking heatwaves caused a surge in cooling and air conditioning loads, pushing power system demand to unprecedented levels and placing immense stress on grid operations [3].

Extreme heat significantly intensifies grid pressure by increasing temperature-controlled loads to peak levels and reducing the efficiency of key components, such as thermal power plants, transformers, and transmission lines [4]. Multi-

energy complementary systems, which integrate diverse energy sources with flexible scheduling of storage systems, offer a highly promising and innovative solution to enhance both the reliability and long-term stability of power systems under such extreme climatic conditions [5].

Despite the advancements in renewable energy and multi-energy complementary systems (MECS) research, critical gaps remain in addressing the resilience and operational optimization of these systems, particularly under extreme heat conditions. First, there is a lack of studies on large-scale MECS, and few publications address the optimization of scheduling strategies or the quantification of resilience in these systems [6]. Second, existing studies primarily focus on conventional operational scenarios, overlooking the risks posed by extreme weather events in recent years. Finally, although some studies have explored system reliability and stability, quantitative analyses of the resilience impacts of extreme heat on power systems are insufficient. This gap has led to a lack of effective methods for enhancing the resilience of power systems under extreme climatic conditions [7]. Although MECS improve system stability and flexibility, their potential to mitigate extreme heat impacts and enhance resilience remains underexplored.

This study aims to address these critical gaps by developing optimized scheduling strategies and a resilience evaluation framework for MECS under extreme heat conditions. By comprehensively accounting for complex operational factors, the proposed approach provides theoretical foundations and practical methodologies to enhance power system stability and robustness, particularly during extreme heat events.

Extreme heat not only leads to surging power demand and intensified supply pressure but also significantly reduces the efficiency and reliability of power system equipment. Specifically, the demand for temperature-controlled loads increases sharply during high-temperature conditions, creating unprecedented operational challenges for power systems. Qiao et al. observed that during heatwaves, temperature-controlled equipment demands surge, leading to record-breaking power loads and heightened grid stress [8]. Concurrently, the operational efficiency of power equipment declines markedly in high-temperature environments [9, 10]. For instance, Ke et al. [11] demonstrated that high temperatures reduce the cooling efficiency of thermal power plants, while Li et al. [12] showed that PV module efficiency decreases significantly under high temperatures due to their sensitivity to temperature variations. Additionally, wind power generation can be adversely affected when reduced wind speeds exacerbate supply instability during extreme heat.

The rapid development of renewable energy in recent years has positioned MECS as a critical approach to improving the stability, flexibility, and economic efficiency of power systems [13]. By coordinating diverse energy sources such as wind, solar, and hydro with flexible energy storage, MECS enhance adaptability and resilience [14, 15]. They leverage the complementary characteristics of these energy sources, bolstering regulatory capabilities under normal conditions and playing a vital role in extreme climates. However, most existing studies on MECS optimization focus on conventional weather conditions, offering limited insight into their performance under extreme heat [6, 14-18].

Recent research has explored the complementary nature of diverse energy sources for power balancing. For instance, studies have highlighted the significant complementarity among water flow, wind speed, and solar radiation under climate change scenarios, enhancing reliability and reducing curtailment risks [19]. Coordinated scheduling models for wind-solar-thermal-pumped-storage systems emphasize the complementary capabilities of generation units in terms of speed and capacity regulation [6].

As the focus on extreme weather conditions increases, the impact of extreme heat on power systems has become a research priority. For example, a long-term hydro-wind-solar complementary scheduling model was developed to improve grid resilience under extreme drought conditions, achieving maximum generation and storage objectives [20]. However, this model did not consider the interplay between drought and heatwaves or the limitations of short-term operations. Another study demonstrated the effectiveness of pumped hydro storage systems in mitigating duck-shaped net load curves and supporting renewable energy integration in regions with high renewable energy penetration [16].

Tan et al. [7] developed a wind-solar-hydro-storage scheduling model to evaluate the trade-offs of various load strategies, addressing risks and uncertainties in MECS. Although joint operation strategies improved reliability, they introduced risks related to reservoir management and grid operation. A two-stage optimization scheduling strategy was proposed to address uncertainties in wind and solar power forecasting and load demand [21]. Additionally, a three-stage scheduling model for wind-solar-hydro complementary systems considering forecast uncertainties was shown to enhance average generation and reduce curtailment rates [22].

Comprehensive optimization studies have focused on achieving economic and environmental balance in wind-solar-thermal systems, enhancing renewable energy utilization [23]. Similarly, research on mixed power systems comprising wind, solar, hydro, thermal, and pumped storage units has highlighted the role of pumped hydro storage in improving system security [17]. Despite these advancements, the impact of extreme heat on power system scheduling remains underexplored. For instance, a study on Sichuan's extreme heat and drought conditions proposed a multi-objective scheduling model integrating hydro-wind-solar-storage systems, emphasizing reserve capacity, flexible transmission contracts, and demand response mechanisms [3]. While these studies provide theoretical insights for scheduling optimization, they leave a gap in understanding the specific impacts of extreme heat on MECS.

To address these gaps, this paper introduces a comprehensive scheduling strategy for MECS, emphasizing both system resilience and operational efficiency under extreme heat conditions. The key contributions are as follows:

- Develops an innovative scheduling framework for MECS, systematically addressing load fluctuations, efficiency degradation, and reduced transmission capacity, ensuring robust system performance under extreme heat conditions.
- Designs a demand response and load shedding strategy to enhance system flexibility and emergency response capabilities.
- Applies the Combined Analytic Hierarchy Process-Entropy Resilience Evaluation (CAHP-ERE) method to evaluate the reliability, safety, and flexibility of MECS, offering a comprehensive resilience assessment.

The paper is organized as follows: Section II models the impacts of extreme heat on MECS. Section III introduces the load shedding strategy, demand response implementation, and resilience evaluation using the CAHP-ERE method. Section IV presents the MECS scheduling optimization model. Section V discusses a case study with comparative analysis. Section VI concludes the paper and outlines future research directions. The research framework is shown in Fig. 1.

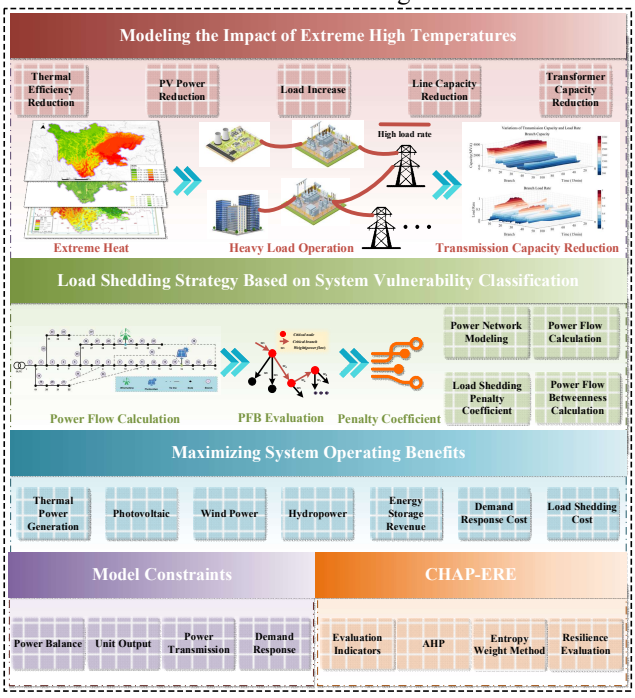

Fig. 1. Research framework of this paper.

## II. Modeling the Impact of Extreme Heat

### A. Efficiency Degradation Models

PV modules exhibit a negative temperature coefficient, indicating a decrease in photoelectric conversion efficiency as operating temperature exceeds the standard threshold. Under extreme heat conditions, this effect on PV efficiency becomes particularly pronounced. To quantitatively describe this impact, Eq. (1) models the PV power output considering radiation intensity and temperature effects [10]:

$$P_t^{\mathrm{PV}} = P^{0,\mathrm{PV}} \frac{I_t}{I^0}[1-\delta_p(T_t^{\mathrm{PV}} - T^{0,\mathrm{PV}})] \tag{1}$$

$$T_t^{\mathrm{PV}} = c_1 + c_2 \cdot T_t^{\mathrm{air}} + c_3 \cdot I_t + c_4 \cdot v_t \tag{2}$$

$$z_{i,j}^{ewe} = \begin{cases} 1, & T_{i,j} \le T_{health\_air} \\ 1-\rho\cdot(T_{i,j} - T_{health\_air}), & T_{i,j} \ge T_{health\_air} \end{cases} \tag{3}$$

Eq. (1) defines the power output calculation for PV modules, while Eq. (2) models their actual operating temperature under varying conditions. For thermal power plants equipped with closed-loop cooling systems, increases in ambient temperature result in a direct decline in generator efficiency [11]. The power generation efficiency of thermal unit $i$ at time $j$ is mathematically represented by the piecewise linear function provided in Eq. (3) [10].

### B. Modeling the Impact on Load and Transmission Infrastructure

Electricity demand exhibits high sensitivity to weather conditions, with temperature fluctuations exerting a direct influence on power load. To quantify this relationship, the power demand model under extreme weather conditions is formulated in Eq. (4) [10]:

$$Load_j^{ewe} = Load_j + C^l \cdot \left(T_j - T_j^{ref}\right) \tag{4}$$

In power systems, the reliability of transmission infrastructure is paramount, particularly for large oil-immersed transformers, which serve as critical components within the grid. Unexpected incidents or transformer overloads can result in outages, leading to extensive power disruptions or blackouts, causing significant economic losses and societal impacts. Research indicates that transformer load capacity decreases markedly under extreme heat conditions [24]. Drawing on the findings of G. W. Swift et al. [25], this paper adopts a heat-induced transformer load capacity reduction model to quantify the impact of high temperatures on transformer performance.

The relationship between transmission line capacity and temperature rise is captured through a thermal balance equation, incorporating factors such as conductor heat generation, radiative cooling, convective cooling, and solar heat absorption. This relationship is mathematically represented in Eq. (5) [26]:

$$I = \sqrt{\frac{W_R + W_F - W_S}{R_t^{'}}} \tag{5}$$

Eq. (5) is formulated under the assumption of steady-state thermal conditions in transmission lines, taking into account key factors such as convective and radiative cooling.

Notably, while high temperatures and drought events significantly affect most power generation facilities, wind turbines remain largely unaffected due to their minimal reliance on external cooling water systems during operation. Consequently, extreme drought conditions have a negligible impact on wind power generation. Furthermore, wind turbines are designed to operate within a broad temperature range of −20 °C to 50 °C, making the influence of extreme heat on their performance insignificant [10].

## III. Load Management and System Resilience Evaluation

### A. Demand Response

Incentive-based emergency demand response measures are crucial regulatory tools in power system operations [27]. This paper primarily focuses on incentive-driven demand response loads, which include two main categories: shiftable loads and curtailable loads [28]. Shiftable loads are highly controllable and generally non-interruptible. However, their operation can be shifted entirely within specific time frames, such as electric vehicle charging and industrial loads. Curtailable loads, on the other hand, are loads that can be temporarily disconnected or reduced during grid emergencies, such as temperature-controlled loads and lighting systems. The models for these loads are presented as follows:

$$C_{shift} = \sum_{t=1}^{T}\sum_{i=1}^{N_{bus}} c_{shift} P_{i,t}^{shift} \tag{6}$$

$$C_{int} = \sum_{t=1}^{T}\sum_{i=1}^{N_{bus}} c_{int} P_{i,t}^{int} \tag{7}$$

$$P_t^{int} = \sum_{i=1}^{N} U_{i,t} S_{i,t} \tag{8}$$

Eq. (6) represents the subsidy cost model for shiftable loads. Eq. (7) and Eq. (8) define the subsidy cost models for curtailable loads.

### B. Load Shedding with Graded Reduction

Under extreme conditions such as power shortages or equipment failures, it is crucial to implement targeted load shedding to ensure the core functionality and overall stability of the power system [29]. A graded load shedding strategy can sequentially reduce loads based on the importance and vulnerability of each node, preventing system collapse. This approach helps the power system maintain essential operations during adverse conditions, reduce economic and operational losses, and expedite subsequent recovery efforts.

To comprehensively evaluate the importance of each node in the grid, all "source-load" combinations passing through a node must be considered. Based on the characteristics of power flow propagation in the system, this study defines Node Power Flow Betweenness (NPFB), incorporating maximum transferable power, to quantify the importance of nodes within the system. The calculation of NPFB is shown as follows [30]:

$$NPFB(l) = \sum_{g\in G}\sum_{d\in D} \min(P_g, P_d)\frac{P_{gd}(n)}{P_{gd}} \tag{9}$$

where $\min(P_g, P_d)$ represents the weight factor for a single power flow betweenness, denoting the smaller value between the actual output of source $g$ and the actual power of load $d$, indicating the maximum transferable power between the source and load. $P_{gd}(n)$ is the active power transmitted between source $g$ and load $d$ via node $n$, while $P_{gd}$ is the total active power transmitted from source $g$ to load $d$. $G$ and $D$ represent the sets of sources and loads, respectively. As NPFB is related not only to the actual output of sources and loads but also reflects the system's operational state and network topology, this measure effectively captures the contribution and importance of nodes in power transmission, serving as a valuable metric for identifying vulnerable nodes [31].

As shown in Fig. 2, the vulnerability analysis of the IEEE 30-bus system, highlighting nodes with critical power flow significance. The graded load shedding strategy incorporates vulnerability-weighted penalties based on identified system vulnerabilities. This prioritizes the protection of critical nodes, ensuring stability during optimization scheduling under extreme conditions.

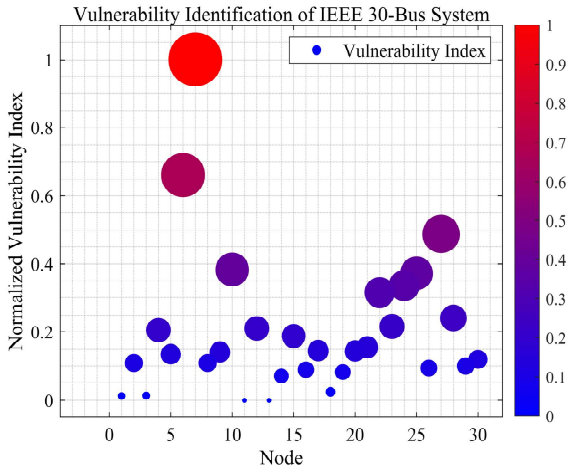


Fig. 2. Vulnerability identification results of the IEEE 30-bus system.

### C. Resilience Evaluation Method for MECS

To thoroughly assess the resilience of MECS under various scenarios, this paper introduces the CAHP-ERE method [32]. This method integrates subjective and objective weighting mechanisms, offering a balanced and robust approach for evaluating the resilience of complex systems like MECS under extreme climatic conditions. Specifically, Analytic Hierarchy Process (AHP) is employed to determine the subjective weights of the evaluation criteria, while the Entropy Weight Method (EWM) is used to calculate objective weights. By combining these two methods, the CAHP-ERE ensures a comprehensive assessment, making it well-suited for systems with multiple evaluation criteria [33].

In the CAHP-ERE process, AHP assigns subjective weights to evaluation criteria, yielding a weight matrix of [0.2, 0.5, 0.1, 0.1, 0.1]. EWM subsequently determines the objective weights, resulting in an entropy weight matrix of [0.1891, 0.1915, 0.1831, 0.2614, 0.1748]. These weights are then integrated with equal importance (50% each), producing the final resilience evaluation results.

The resilience evaluation process considers several key performance indicators, including the average load rate of critical transmission lines, load shedding volume, rated capacity of thermal power units, peak-to-valley difference, and peak regulation margin. These indicators provide a quantifiable framework for evaluating MECS reliability, adaptability, and flexibility under challenging conditions.

## IV. MECS Optimization Scheduling Model

### A. Objective Function

The goal of the MECS optimization is to maximize overall system profit by efficiently allocating energy resources under extreme heat conditions. The optimization model incorporates revenues from various energy sources, penalties for renewable energy curtailment, and demand response incentives to strengthen system resilience and operational efficiency. The mathematical representation of the MECS objective function is as follows:

$$\max \quad F = P_g + P_w + P_v + P_h + P_{ESS} - C_{DR} - C_{shed} \tag{10}$$

$$P_{ESS} = I_{ESS} - C_{ESS} \tag{11}$$

$$I_{ESS} = \sum_{t=1}^{T}(p_t^{grid} P_t^{dis} \eta_{\mathrm{d}} - \frac{p_t^{grid} P_t^{char}}{\eta_{\mathrm{c}}})\Delta t \tag{12}$$

$$C_{ESS} = \sum_{t=1}^{T} c_{ESS}\left(P_t^{dis} + P_t^{dis}\right)\Delta t \tag{13}$$

$$P_g = I_g - C_g \tag{14}$$

$$I_g = \sum_{t=1}^{T}\sum_{i=1}^{N_G} P_{i,t}^g p_t^{grid} \Delta t \tag{15}$$

$$C_g = C_{coal} + C_{ss} \tag{16}$$

$$C_{coal} = \sum_{t=1}^{T}\sum_{i=1}^{N_g} C_{i,t,coal}\Delta t \tag{17}$$

$$C_{i,t,coal} = a_i\left(P_{i,t}^g\right)^2 + b_i P_{i,t}^g + c_i U_{i,t}^g \tag{18}$$

$$C_{ss} = \sum_{t=2}^{T}\sum_{i=1}^{N_g}[S_{i,\mathrm{start}} U_{i,t}^g\left(1 - U_{i,t-1}^g\right) + S_{i,\mathrm{stop}} U_{i,t-1}^g\left(1 - U_{i,t}^g\right)] \tag{19}$$

$$P_w = \sum_{t=1}^{T}(p_w P_t^w - \theta_w P_{t,cur}^w)\Delta t \tag{20}$$

$$P_v = \sum_{t=1}^{T}(p_v P_t^v - \theta_v P_{t,cur}^v)\Delta t \tag{21}$$

$$P_h = \sum_{t=1}^{T}(p_h P_t^h - \theta_h P_{t,cur}^h)\Delta t \tag{22}$$

$$C_{DR} = C_{shift} + C_{int} \tag{23}$$

$$C_{shed} = \sum_{t=1}^{T}\sum_{i=1}^{N_{bus}} P_{i,t}^{shed} p_{i,t}^{shed} c_{i,t}^{shed} \tag{24}$$

In the MECS optimization scheduling model, Eq. (10) represents the objective function, which comprises the cost and revenue models of various energy components. Eqs. (11)-(13) describe the operating revenue and cost model of the energy storage system, which accounts for energy losses during charging and discharging processes. Eqs. (14)-(19) model the operating revenue and costs of thermal power units, mainly including the revenue from electricity sales and the costs associated with fuel consumption and startup/shutdown operations. Eqs. (20)-(22) describe the revenue models of clean energy units, which encompass not only electricity sales but also penalties for curtailing renewable energy. Eq. (23) formulates the subsidy cost model for demand response, covering the costs associated with shiftable and curtailable loads. Eq. (24) models the penalty costs for direct load shedding, weighted by the system vulnerability at each node.

### B. Constraints

The constraints in the model are categorized into three types: 1) generation units and energy storage system constraints; 2) grid and power balance constraints; and 3) reserve and demand response constraints.

*1) Generation Units and Energy Storage System Constraints*

$$0 \le P_t^w \le P_{t,\max}^w \tag{25}$$

$$0 \le P_t^v \le P_{t,\max}^v \tag{26}$$

$$0 \le P_t^h \le P_{t,\max}^h \tag{27}$$

$$U_{i,t}^g P_{i,\min}^g \le P_{i,t}^g \le U_{i,t}^g P_{i,\max}^g \tag{28}$$

$$-r_{i,down} \le P_{i,t} - P_{i,(t-1)} \le r_{i,up} \tag{29}$$

$$S_t^{ESS} = S_{t-1}^{ESS}(1-\delta) + \frac{P_t^{char}\eta_{\mathrm{c}}\Delta t}{E_{ESS}} - \frac{P_t^{dis}\Delta t}{\eta_d E_{ESS}} \tag{30}$$

$$S_{\min} \le S_t^{ESS} \le S_{\max} \tag{31}$$

$$S_T^{ESS} = S_0^{ESS} \tag{32}$$

$$U_t^{char} P_{\min}^{char} \le P_t^{char} \le U_t^{char} P_{\max}^{char} \tag{33}$$

$$U_t^{dis} P_{\min}^{dis} \le P_t^{dis} \le U_t^{dis} P_{\max}^{dis} \tag{34}$$

$$U_t^{char} + U_t^{dis} \le 1 \tag{35}$$

Eqs. (25)-(28) represent the output constraints for generation units, and Eq. (29) describes the ramp rate constraints for thermal power units. Eqs. (30)-(35) define the energy constraints and charge/discharge constraints for the energy storage system, ensuring the state of charge at the start and end of the scheduling period remains equal.

*2) Grid and Power Balance Constraints*

$$\left|B_{i,j}\left(\theta_{i,t} - \theta_{j,t}\right)\right| \le \alpha_{t,l}^{temp}\beta_{t,tr}^{temp} P_{i,j,\mathrm{Lmax}} \tag{36}$$

$$\sum_{i=1}^{N_g} P_{i,t}^g + P_t^w + P_t^v + P_t^h + P_t^{dis} + P_t^{char} = \sum_{i=1}^{N_{bus}} P_{i,t}^L + \sum_{i=1}^{N_{shift}}\left(P_{i,t,\mathrm{in}}^{shift} - P_{i,t,\mathrm{out}}^{shift}\right) - \sum_{i=1}^{N_{int}} P_{i,t}^{int} - \sum_{i=1}^{N_{shed}} P_{i,t}^{shed} \tag{37}$$

Eq. (36) specifies the transmission capacity constraints, with upper and lower bounds varying with temperature [34]. When a line operates at its rated temperature, the coefficient $\alpha_{t,l}^{temp}$ equals 1. Similarly, $\beta_{t,l}^{temp}$ equals 1 when the transformer is at normal operating temperature or when there is no transformer between nodes $i$ and $j$. Eq. (37) ensures the power and energy balance across the system at all times.

*3) Reserve and Demand Response Constraints*

$$P_{i,t,\max}^g - P_{i,t}^g \ge \lambda \sum_{i=1}^{N_{bus}} P_{i,t}^L \tag{38}$$

$$\sum_{t=1}^{T} P_{i,t,in}^{shift} = \sum_{t=1}^{T} P_{i,t,out}^{shift} \tag{39}$$

$$0 \le P_{i,t}^{shift} \le P_{i,t,\max}^{shift} \tag{40}$$

$$0 \le P_{i,t}^{int} \le P_{i,t,\max}^{int} \tag{41}$$

Eq. (38) defines the reserve constraints, where the reserve ratio is determined based on system security, load fluctuations, and unit reliability [35]. Eqs. (39)-(41) specify the demand

response constraints, ensuring that the total load before and after demand response at each node remains constant throughout the scheduling period [36].

## V. Case Study

### A. Data and Parameters

This study constructs a simulation model for a provincial power grid based on the IEEE 30-bus system [37], including power composition and unit distribution. The system topology is illustrated in Fig. 3. The simulation model comprises two thermal power plants, one hydropower station, a wind farm with a total capacity of 150 MW, and a PV plant with a total capacity of 150 MW. The capacity configuration of the energy storage system follows the optimal configuration scheme without considering investment costs and employs modular lithium iron phosphate batteries. The basic parameters of the thermal power plants, the hydropower station, and the energy storage system are provided in Table I. The system's spinning reserve capacity is set to 6% of the load [38]. The grid electricity price for thermal power is \$51.64/MWh, while the benchmark prices for wind and PV are \$55.25/MWh. The penalty coefficients for curtailed wind and PV power are \$137.71/MWh [39]. The base penalty cost for load shedding is \$1,000/MWh [40]. For demand response, the subsidy costs for curtailable and shiftable loads are \$297.81/MWh and \$140.5/MWh, respectively [41]. The case study data is derived from a high-renewable-energy penetration regional power system, encompassing hydrological data, temperature fluctuations, and load variation information under extreme high-temperature conditions.

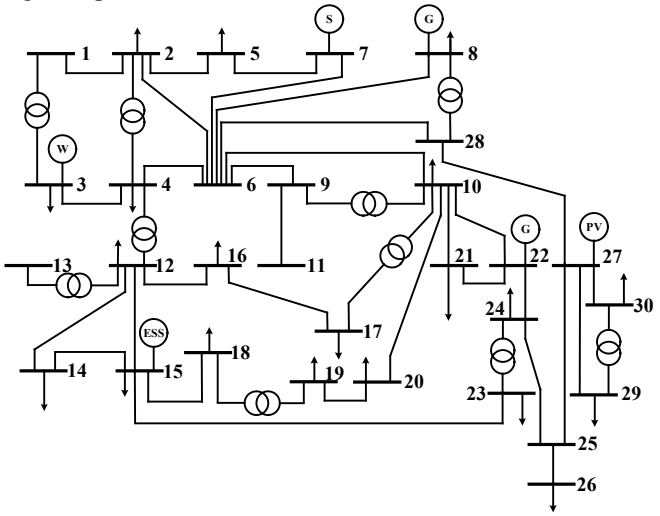


Fig. 3. Modified IEEE 30-bus system [37].

To validate the proposed model, this study tested the optimization scheduling results of the multi-energy complementary system across 96 intraday periods. The model was implemented on the MATLAB 2022a platform, utilizing the YALMIP interface to invoke the CPLEX 12.10 solver. Simulations were conducted on a computer equipped with an AMD Ryzen 5 4500 processor and 16 GB of RAM, with the maximum simulation runtime recorded at 32.4 seconds..

### B. Results and Analysis

This study defines five distinct scenarios to evaluate the performance of MECS under varying external conditions. Scenario 1 serves as the baseline, representing normal operating conditions to validate the overall effectiveness and accuracy of the proposed model. Scenario 2 incorporates extreme heat impacts, with a focus on analyzing the sensitivity of PV generation to temperature variations and the degradation of thermal power efficiency, while assessing system adaptability under high-temperature environments. Scenario 3 examines power shortage scenarios, simulating scheduling responses to investigate resource coordination strategies under constrained supply conditions. Scenario 4 considers the combined impacts of extreme heat and power shortages, emphasizing the compounded challenges posed to system operation and resource management. Building upon Scenario 4, Scenario 5 introduces demand response mechanisms to evaluate their effectiveness in optimizing scheduling and enhancing system performance under complex and adverse conditions. The key objectives and results for each scenario are summarized in Table II, while detailed scheduling outcomes are illustrated in Fig. 4.

TABLE I Parameters of Thermal Power Plants, Hydropower Plant, and ESS

| Device Type | Parameter | Value | Unit |
|---|---|---|---|
| Thermal Power Plant 1 | Upper Output Limit | 800 | MW |
| | Lower Output Limit | 400 | MW |
| | Reserve capacity | 48 | MW |
| | Ramp Rate | 400 | MW/h |
| | Fuel Cost Coefficients $a_i$ | 0.0211 | \$/(MW)² |
| | Fuel Cost Coefficients $b_i$ | 21.05 | \$/MW |
| | Fuel Cost Coefficients $c_i$ | 1313.6 | \$ |
| Thermal Power Plant 2 | Upper Output Limit | 1200 | MW |
| | Lower Output Limit | 600 | MW |
| | Reserve capacity | 72 | MW |
| | Ramp Rate | 600 | MW/h |
| | Fuel Cost Coefficients $a_i$ | 0.07 | \$/(MW)² |
| | Fuel Cost Coefficients $b_i$ | 23.9 | \$/MW |
| | Fuel Cost Coefficients $c_i$ | 471 | \$ |
| Hydro-power Plant | Installed Capacity | 4500 | MW |
| | Minimum Operating Water Level | 370 | m |
| | Rated Water Head | 104 | m |
| | Maximum Release Flow Rate | 7740 | $m^3/s$ |
| | Maximum Overflow Flow Rate | 9000 | $m^3/s$ |
| | Initial Adjustable Capacity | $21.5\times10^9$ | $m^3$ |
| | Maximum Adjustable Capacity | $49.8\times10^9$ | $m^3$ |
| | Head Loss | 2 | m |
| ESS | Storage Capacity | 800 | MW·h |
| | Maximum Charge/Discharge Power | 400 | MW |
| | Upper/ Lower State of Charge | 0.9/0.1 | — |
| | Charging/Discharging Efficiency | 0.9 | — |
| | Initial charge status | 0.5 | — |

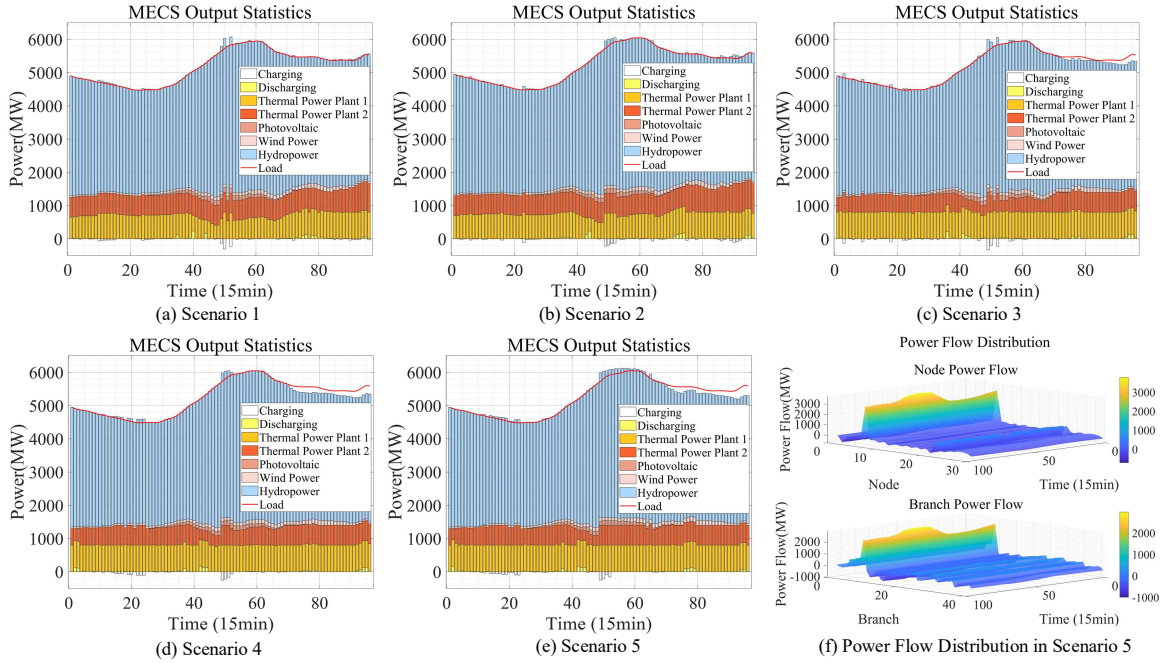


Fig. 4. Optimization scheduling results of MECS in 5 scenarios.

TABLE II OPTIMIZATION RESULTS AND SCENARIO COMPARISON: SYSTEM PERFORMANCE UNDER EXTREME CONDITIONS

| | Scenario 1 | Scenario 2 | Scenario 3 | Scenario 4 | Scenario 5 |
|---|---|---|---|---|---|
| Extreme Heat | — | √ | — | √ | √ |
| Power Shortage | — | — | √ | √ | √ |
| Thermal Efficiency Degradation | — | √ | — | √ | √ |
| Demand Response | — | — | — | — | √ |
| Hierarchical Load Shedding | — | — | √ | √ | √ |
| Peak Load (MW) | 5949.4 | 6045.8 | 5949.4 | 6045.8 | 6045.8 |
| Rated Thermal Capacity (MW) | 2000 | 2000 | 1400 | 1400 | 1400 |
| Maximum PV Output (MW) | 150 | 140.25 | 150 | 140.25 | 140.25 |
| Unit Thermal Profit ($/MWh) | 6.22 | 4.25 | 7.68 | 6.1 | 6.07 |
| Avg. Load Rate of Key Branches | 0.4139 | 0.5163 | 0.4111 | 0.5116 | 0.5133 |
| Direct Load Shedding (MWh) | 0 | 0 | 562.68 | 1059 | 558.98 |
| Shiftable/Curtailable Load (MW) | — | — | — | — | 200/300 |
| Peak-Valley Difference (MW) | $1.4780\times10^3$ | $1.5672\times10^3$ | $1.4780\times10^3$ | $1.5672\times10^3$ | $1.5151\times10^3$ |
| Total Profit ($) | $5.7340\times10^6$ | $5.5017\times10^6$ | $5.2915\times10^6$ | $4.5653\times10^6$ | $5.0282\times10^6$ |
| Peak-Shaving Margin | 0.1307 | 0.1180 | 0.0196 | 0.0120 | 0.0096 |
| Resilience Evaluation | 1 | 0.9118 | 0.5112 | 0.2 | 0.4329 |

*1) Impact of Extreme Heat on the System*: Comparing Scenario 1 and Scenario 2, extreme heat significantly increases system operation pressure. Specifically, the peak load increases by 1.6%, and the efficiency of photovoltaic modules and thermal power units decreases, resulting in a reduction in unit profit from $6.22/MWh to $4.25/MWh and a total profit decline of 4.1%. Meanwhile, the average load rate of critical lines rises, reflecting increased system carrying pressure. The resilience index drops from 1.0 to 0.9118, indicating that extreme heat undermines system stability and safety, increasing operational risks.

*2) Impact of Power Shortage on the System*: While Scenario 2 focuses on the impacts of extreme heat, Scenario 3 shifts the focus to power shortages, revealing how constrained generation capacity exacerbates system vulnerabilities.A comparison of Scenario 1 and Scenario 3 reveals the significant impact of power shortages on the system. Insufficient thermal power capacity leads to direct load shedding of 562.68 MWh, resulting in a 7.7% decline in total profit. Nevertheless, due to the improved utilization rate of thermal power units, the unit profit rises from $6.22/MWh to $7.68/MWh, indicating that the economic benefits of thermal power units are enhanced under power shortage conditions. However, the resilience index decreases to 0.5112, reflecting a significant reduction in system stability and adaptability.

*3) Synergistic Effects of Extreme Heat and Power Shortages*: Building on the individual impacts observed in Scenarios 2 and 3, Scenario 4 highlights the compounded challenges posed by concurrent extreme heat and power shortages.The comparison between Scenario 1 and Scenario 4 further

demonstrates the profound impact of combined pressure from extreme heat and power shortages on the system. Peak load growth, thermal power efficiency reduction, and direct load shedding reach 1059 MWh, intensifying the imbalance between supply and demand. Total profit declines by 20.4%, peak-shaving capacity drops to 0.0120, and flexibility is nearly lost. The resilience index falls to 0.2, indicating that the system is close to operational limits with significant deficiencies in safety and adaptability.

*4) Optimization Effects of Demand Response and Load Shedding Strategies*: A comparison of Scenario 4 and Scenario 5 highlights significant performance improvements following the introduction of demand response and load shedding strategies. Direct load shedding reduces to 558.98 MWh, representing a 47.2% optimization. Demand response prioritizes reducing non-critical loads and shifts part of the load to off-peak periods, effectively optimizing load distribution and alleviating peak operating pressure. This increases total profit from $\$4.5653\times10^6$ to $\$5.0282\times10^6$, a rise of 10.1%. The resilience index improves from 0.2 to 0.4329, achieving a 116.5% increase and significantly enhancing system safety and adaptability. The demand response and load shedding strategies effectively prioritize critical loads while alleviating peak pressure through load redistribution. This ensures that the system maintains stability and achieves economic efficiency, even under extreme heat and power shortage conditions.

The primary negative impacts of extreme heat and power shortages on the system include increased load pressure, reduced equipment efficiency, diminished flexibility, and lower economic benefits. In contrast, demand response and load shedding strategies significantly optimize load distribution, reduce load shedding, enhance system profitability and resilience, and demonstrate remarkable effectiveness in addressing complex operating conditions of power systems.

### *C. Discussion*

As shown in Fig. 4(f), the power flow analysis of Scenario 5 reveals that Branch 9, a critical branch connecting the hydropower station to the MECS, carried a transmission load of 2978.2 MW during peak periods. However, extreme heat significantly increased the branch's load, drastically raising its operational pressure and posing a severe challenge to the safe and stable operation of the grid.

As illustrated in Fig. 5, during the 12:00–17:00 time period, under extreme heat conditions (Scenarios 2, 4, and 5), Branch 9 operated dangerously close to its full capacity. In stark contrast, under normal temperature conditions (Scenarios 1 and 3), the maximum load rate of the branch reached only 76.7%. The high-temperature conditions significantly raised the load rate of this critical branch by approximately 25%, further worsening the peak-valley difference and amplifying the demand for thermal power output. With the intensification of power shortages and the continued escalation in load, the system's already limited peak-shaving margin was further compressed. Notably, under extreme heat conditions, the dramatically reduced peak-shaving margin rendered the system increasingly fragile and vulnerable to operational risks.

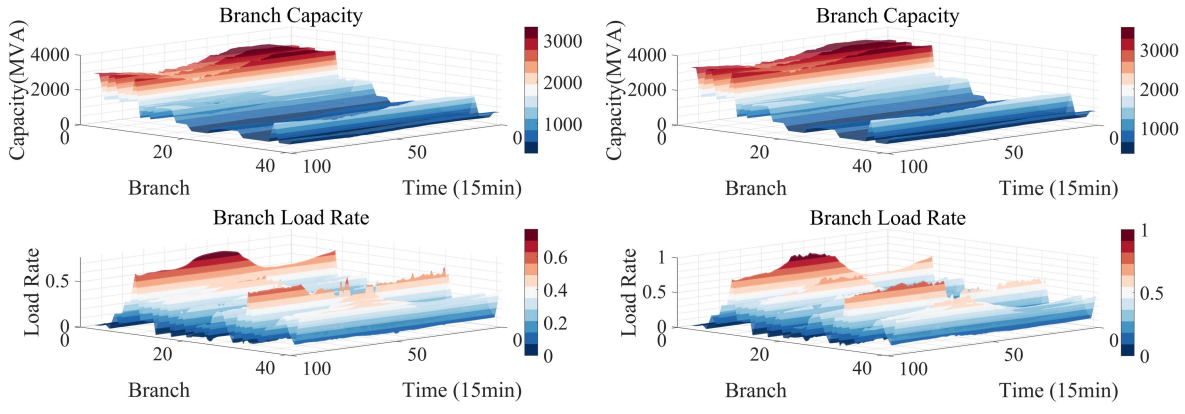


(a) Scenario 3 (b) Scenario 5

Fig. 5. Comparison of Power Flow Transmission Capacity of MECS in Scenarios 3 and 5.

As illustrated in Fig. 6, in Scenario 3, power shortages resulted in a substantial amount of load shedding, making it difficult to effectively meet peak load demands. In Scenario 4, with the addition of extreme heat conditions, the load shedding volume nearly doubled, intensifying the supply-demand imbalance. Extreme heat not only significantly reduced the grid's load-bearing capacity—especially the capacity of transmission branches and transformers—but also further aggravated the system's vulnerability due to sustained load increases. Additionally, the energy storage system, limited by its power and capacity constraints, struggled to provide sufficient electricity through temporal and spatial energy transfers.

In Scenario 5, the introduction of demand response strategies markedly enhanced the system's peak-shaving capability. By negotiating agreements with users on curtailable and shiftable loads, Scenario 5 effectively optimized load management. This not only substantially reduced the system's peak-valley difference but also fully leveraged the energy potential of the system. In this scenario,

a portion of the peak-period load was shifted to off-peak periods, effectively alleviating the supply-demand imbalance under high-temperature conditions. A comparative analysis of load shedding indicates that, in all scenarios, high-vulnerability nodes (top 15 ranked nodes in vulnerability) experienced no load shedding at any time. This demonstrates that the flexible scheduling strategy targeting high-vulnerability nodes effectively avoided load reductions at these critical nodes, thereby enhancing the system's risk resilience and the stability of load reductions.

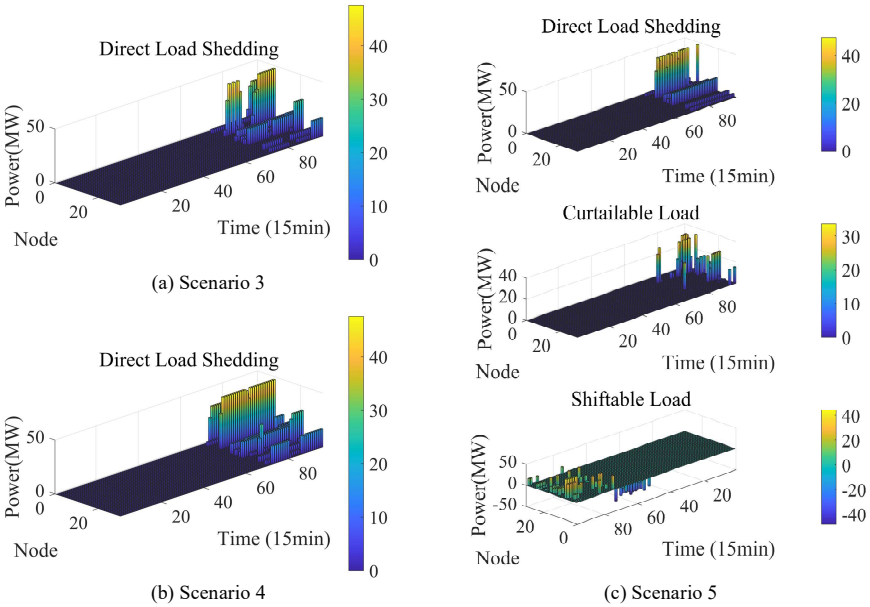


(a) Scenario 3

(b) Scenario 4

(c) Scenario 5

Fig. 6. Comparison of load shedding in Scenarios 3, 4, and 5: Assessing the effect of demand response and load management strategies.

The impact of extreme heat and power shortages on the optimization and scheduling of MECS is notably significant. In MECS, the optimization of system scheduling and load management is especially critical. By introducing demand response and load shedding strategies, the system's peak-shaving flexibility and resilience can be effectively improved, ensuring the stability of power supply under extreme heat and power shortage conditions.

## VI. Conclusion

This study explores the optimization scheduling and resilience quantification of MECS under extreme high-temperature conditions. It addresses critical challenges such as surging load demand, diminished generation efficiency, and reduced transmission capacity. A regional grid-based case study was conducted to validate the proposed approaches. The key findings are summarized as follows:

*1) Impact Modeling and Optimization*: The study incorporates the effects of extreme heat on electricity demand, generation efficiency, and transmission capacity. A comprehensive high-temperature impact model was developed, providing theoretical and practical support for the scientific optimization of MECS scheduling.

*2) Risk Mitigation through Vulnerability-Based Load Management*: A load-shedding strategy based on vulnerability analysis prioritizes critical nodes, enhancing system stability and adaptability under extreme conditions. Combined with demand response mechanisms, the strategy effectively reduces peak demand pressure and enhances resilience.

*3) Resilience Quantification and Validation*: The application of the CAHP-ERE method quantitatively evaluates the reliability, safety, and flexibility of MECS. Results show that demand response and optimized scheduling significantly enhance system resilience, increasing the resilience index from 0.2 to 0.4329, thereby demonstrating improved adaptability to extreme heat conditions.

In conclusion, the proposed MECS optimization scheduling and resilience quantification methods provide critical theoretical and technical support for addressing power supply issues in energy systems under extreme climate conditions. However, the long-term persistence of extreme climate events has not been fully considered. Future research should explore the optimization scheduling of MECS under prolonged extreme climate conditions and conduct more comprehensive assessments and improvements of system resilience to address increasingly complex power system operational environments.

## References

[1] J. Zhao, F. Li, and Q. Zhang, “Impacts of renewable energy resources on the weather vulnerability of power systems,” *Nature Energy,* vol. 9, no. 11, pp. 1407-1414, 2024.

[2] A. Dewan. "This summer was Europe’s hottest on record as Mediterranean heat soared," https://edition.cnn.com/2021/09/07/europe/europe-hottest-summer-climate-intl/index.html.

[3] S. Zhou, Y. Han, A. S. Zalhaf, S. Chen, T. Zhou, P. Yang, and B. Elboshy, “A novel multi-objective scheduling model for grid-connected hydro-wind-PV-battery complementary system under extreme weather: A case study of Sichuan, China,” *Renewable Energy*, pp. 818-33, /, 2023.

[4] M. Choobineh, A. Speake, M. Harris, P. C. Tabares-Velasco, and S. Mohagheghi, “End-User-Aware Community Energy Management in a

Distribution System Exposed to Extreme Temperatures," *IEEE Transactions on Smart Grid,* vol. 10, no. 4, pp. 3753-64, 07/, 2019.
[5] Y. Guo, B. Ming, Q. Huang, P. Liu, Y. Wang, W. Fang, and W. Zhang, "Evaluating effects of battery storage on day-ahead generation scheduling of large hydro-wind-photovoltaic complementary systems," *Applied Energy*, pp. 119781, /, 2022.
[6] X. Shiwei, D. Zhaohao, D. Ting, Z. Dongying, M. Shahidehpour, and D. Tao, "Multitime Scale Coordinated Scheduling for the Combined System of Wind Power, Photovoltaic, Thermal Generator, Hydro Pumped Storage, and Batteries," *IEEE Transactions on Industry Applications,* vol. 56, no. 3, pp. 2227-37, 05/, 2020.
[7] T. Qiaofeng, W. Xin, S. Yuanliang, L. Xiaohui, W. Zhenni, and Q. Guanghua, "Evaluation of the risk and benefit of the complementary operation of the large wind-photovoltaic-hydropower system considering forecast uncertainty," *Applied Energy,* vol. 285, pp. 620-35, 03/01, 2021.
[8] Q. Qiao, Z. Zhang, and B. Lin, "Environmental temperature variation and electricity demand instability: A comprehensive assessment based on high-frequency load situation," *Environmental Impact Assessment Review,* vol. 103, 2023.
[9] D. Burillo, M. V. Chester, S. Pincetl, and E. Fournier, "Electricity infrastructure vulnerabilities due to long-term growth and extreme heat from climate change in Los Angeles County," *Energy Policy,* vol. 128, pp. 943-53, 05/, 2019.
[10] A. F. Abdin, Y. P. Fang, and E. Zio, "A modeling and optimization framework for power systems design with operational flexibility and resilience against extreme heat waves and drought events," *Renewable and Sustainable Energy Reviews,* vol. 112, pp. 706-719, 2019.
[11] X. Ke, D. Wu, J. Rice, M. Kintner-Meyer, and N. Lu, "Quantifying impacts of heat waves on power grid operation," *Applied Energy,* vol. 183, pp. 504-512, 2016.
[12] G. Li, Y. Lu, and X. Zhao, "The Gaussian non-uniform temperature field on PV cells - A unique solution for enhancing the performance of the PV/T module," *Energy,* vol. 250, 2022.
[13] X. Wang, E. Virguez, Y. Mei, H. Yao, and D. Patino-echeverri, "Integrating wind and photovoltaic power with dual hydro-reservoir systems," *Energy Conversion and Management,* vol. 257, pp. 115425, /, 2022.
[14] M. Bo, L. Pan, C. Lei, Z. Yanlai, and W. Xianxun, "Optimal daily generation scheduling of large hydro–photovoltaic hybrid power plants," *Energy Conversion and Management,* vol. 171, pp. 528-40, 2018.
[15] J. Jiang, B. Ming, Q. Huang, J. Chang, P. Liu, W. Zhang, and K. Ren, "Hybrid generation of renewables increases the energy system's robustness in a changing climate," *Journal of Cleaner Production,* vol. 324, 2021.
[16] S. Heng-Yi, L. Jian-Hong, C. Chia-Chi, L. Sheng-Huei, H. Ying-Yi, L. Yu-Jen, and L. Ching-Jung, "Developing an optimal scheduling of taiwan power system with highly penetrated renewable energy resources and pumped hydro storages," *IEEE Transactions on Industry Applications,* vol. 57, no. 3, pp. 1973-86, /, 2021.
[17] F. Yiwei, L. Zongxiang, H. Wei, W. Shuang, W. Yiting, D. Ling, and Z. Jietan, "Research on joint optimal dispatching method for hybrid power system considering system security," *Applied Energy,* vol. 238, pp. 147-63, 03/15, 2019.
[18] Z. Yusheng, M. Chao, L. Jijian, P. Xiulan, Q. Yanan, and E. Chaima, "Optimal photovoltaic capacity of large-scale hydro-photovoltaic complementary systems considering electricity delivery demand and reservoir characteristics," *Energy Conversion and Management,* vol. 195, pp. 597-608, 2019.
[19] Q. Cheng, P. Liu, J. Xia, B. Ming, L. Cheng, J. Chen, K. Xie, Z. Liu, and X. Li, "Contribution of complementary operation in adapting to climate change impacts on a large-scale wind–solar–hydro system: A case study in the Yalong River Basin, China," *Applied Energy,* vol. 325, 2022.
[20] H. Wang, S. Liao, B. Liu, H. Zhao, X. Ma, and B. Zhou, "Long-term complementary scheduling model of hydro-wind-solar under extreme drought weather conditions using an improved time-varying hedging rule," *Energy,* vol. 305, 2024.
[21] S. S. Reddy, "Optimal scheduling of thermal-wind-solar power system with storage," *Renewable Energy,* vol. 101, pp. 1357-68, 02/, 2017.
[22] K. Huang, P. Liu, J. S. Kim, W. Xu, Y. Gong, Q. Cheng, and Y. Zhou, "A model coupling current non-adjustable, coming adjustable and remaining stages for daily generation scheduling of a wind-solar-hydro complementary system," *Energy*, pp. 125737, /, 2023.
[23] X. Jiuping, W. Fengjuan, L. Chengwei, H. Qian, and X. Heping, "Economic-environmental equilibrium based optimal scheduling strategy towards wind-solar-thermal power generation system under limited resources," *Applied Energy,* vol. 231, pp. 355-71, 12/01, 2018.
[24] "IEEE Guide for Loading Mineral-Oil-Immersed Transformers and Step-Voltage Regulators," *IEEE Std C57.91-2011 (Revision of IEEE Std C57.91-1995)*, pp. 1-123, 2012.
[25] G. W. Swift, E. S. Zocholl, M. Bajpai, J. F. Burger, C. H. Castro, S. R. Chano, F. Cobelo, P. de Sa, E. C. Fennell, J. G. Gilbert, S. E. Grier, R. W. Haas, W. G. Hartmann, R. A. Hedding, P. Kerrigan, S. Mazumdar, D. H. Miller, P. G. Mysore, M. Nagpal, R. V. Rebbapragada, M. V. Thaden, J. T. Uchiyama, S. M. Usman, J. D. Wardlow, and M. Yalla, "Adaptive transformer thermal overload protection," *IEEE Transactions on Power Delivery,* vol. 16, no. 4, pp. 516-21, 10/, 2001.
[26] "IEEE Standard for Calculating the Current-Temperature Relationship of Bare Overhead Conductors," *IEEE Std 738-2023 (Revision of IEEE Std 738-2012)*, pp. 1-56, 2023.
[27] Z. Wang, B. Lu, B. Wang, Y. Qiu, H. Shi, B. Zhang, J. Li, H. Li, and W. Zhao, "Incentive based emergency demand response effectively reduces peak load during heatwave without harm to vulnerable groups," *Nature Communications*, pp. 6202 (11 pp.), /, 2023.
[28] X. Sun, H. Xie, Y. Xiao, and Z. Bie, "Incentive compatible pricing for enhancing the controllability of price-based demand response," *IEEE Transactions on Smart Grid*, pp. 418-30, /, 2024.
[29] C. Wang, S. Chu, Y. Ying, A. Wang, R. Chen, H. Xu, and B. Zhu, "Underfrequency Load Shedding Scheme for Islanded Microgrids Considering Objective and Subjective Weight of Loads," *IEEE Transactions on Smart Grid,* vol. 14, no. 2, pp. 899-913, 2023.
[30] L. Chen, S. Gorbachev, D. Yue, C. Dou, X. Xie, S. Li, N. Zhao, and T. Zhang, "Impact of Cascading Failure on Power Distribution and Data Transmission in Cyber-Physical Power Systems," *IEEE Transactions on Network Science and Engineering,* vol. 11, no. 2, pp. 1580-90, /, 2024.
[31] N. Liu, X. Hu, L. Ma, and X. Yu, "Vulnerability Assessment for Coupled Network Consisting of Power Grid and EV Traffic Network," *IEEE Transactions on Smart Grid,* vol. 13, no. 1, pp. 589-598, 2022.
[32] S. Wang, Y. Li, D. Liu, X. Luo, and Y. Sun, "Low-carbon development of urban power grids in China: Quality assessment, obstacle analysis, and potential release," *Energy,* vol. 304, 2024.
[33] Y. Liang, C. Wang, G. Chen, and Z. Xie, "Evaluation framework ACR-UFDR for urban form disaster resilience under rainstorm and flood scenarios: A case study in Nanjing, China," *Sustainable Cities and Society,* vol. 107, pp. 105424, /, 2024.
[34] H. E. House, and P. D. Tuttle, "Current-Carrying Capacity of ACSR," *Transactions of the American Institute of Electrical Engineers. Part III: Power Apparatus and Systems,* vol. 77, no. 3, pp. 1169-1173, 1958.
[35] Y. Xu, L. Yao, T. Pu, S. Liao, F. Cheng, Y. Li, and X. Wang, "Voltage-Dependent P-Q Reserve Capacity Evaluation for TSO-DSO Interface Considering Uncertainties of DGs and FLs," *CSEE Journal of Power and Energy Systems,* vol. 10, no. 5, pp. 1935-54, /, 2024.
[36] H. Wujing, Z. Ning, K. Chongqing, L. Mingxuan, and H. Molin, "From demand response to integrated demand response: review and prospect of research and application," *Protection and Control of Modern Power Systems,* vol. 4, no. 1, pp. 12 (13 pp.), 12/, 2019.
[37] S. Mohammad, and W. Yaoyu, "Appendix C: IEEE30 Bus System Data," *Communication and Control in Electric Power Systems: Applications of Parallel and Distributed Processing*, pp. 493-495: IEEE, 2003.
[38] Y. Liu, Z. Tang, and L. Wu, "On Secured Spinning Reserve Deployment of Energy-Limited Resources Against Contingencies," *IEEE Transactions on Power Systems,* vol. 37, no. 1, pp. 518-529, 2022.
[39] T. Li, Z. Li, J. Yang, D. Cui, Z. Wang, K. Ma, and W. Hu, "Coordination and Optimal Scheduling of Multi-energy Complementary System Considering Peak Regulation Initiative," *Dianwang Jishu/Power System Technology,* vol. 44, no. 10, pp. 3622-3630, 2020.
[40] H. Chuan, Z. Xiaping, L. Tianqi, and W. Lei, "Distributionally Robust Scheduling of Integrated Gas-Electricity Systems With Demand Response," *IEEE Transactions on Power Systems,* vol. 34, no. 5, pp. 3791-803, 2019.
[41] X. Qiao, Z. Yang, Y. Li, F. Ling, J. Zhong, and L. Zhang, "Optimization Strategy for Cooperative Operation of Multi-microgrids Considering Two-level Carbon Trading and Demand Response," *Gaodianya Jishu/High Voltage Engineering,* vol. 48, no. 7, pp. 2573-2589, 2022.